The Role of the Land Surface Background State in Climate Predictability

PAUL A. DIRMEYER

Center for Ocean–Land–Atmosphere Studies, Calverton, Maryland

(Manuscript received 22 July 2002, in final form 20 December 2002)

ABSTRACT

Skill in ensemble-mean dynamical seasonal climate hindcasts with a coupled land–atmosphere model and specified observed sea surface temperature is compared to that for long multidecade integrations of the same model where the initial conditions are far removed from the seasons of validation. The evaluations are performed for surface temperature and compared among all seasons. Skill is found to be higher in the seasonal simulations than in the multidecadal integrations except during boreal winter. The higher skill is prominent even beyond the first month when the direct influence of the atmospheric initial state elevates model skill. Skill is generally found to be lowest during the winter season for the dynamical seasonal forecasts. This is in contrast to the multiyear integrations, which show some of the highest skill during winter—as high as the dynamical seasonal forecasts. The reason for the differences in skill during the nonwinter months is attributed to the severe climate drift in the long simulations, manifested through errors in downward fluxes of water and energy over land and evident in soil wetness. The drift presses the land surface to extreme dry or wet states over much of the globe, into a range where there is little sensitivity of evaporation to fluctuations in soil moisture. Thus, the land–atmosphere feedback is suppressed, which appears to lessen the model's ability to respond correctly over land to remote ocean temperature anomalies. During winter the land surface is largely decoupled from the atmosphere due to increased baroclinic activity in the land-dominated Northern Hemisphere, while at the same time tropical ocean anomalies have their strongest influence. This combination of effects neutralizes the negative impact of climate drift over land during that season and puts all of the climate simulations on an equal footing.

1. Introduction

Prediction of climate anomalies at a lead time of one season or longer is well established as possible and useful, if not completely reliable (Barnston et al. 2000). This is particularly true for the boreal winter season (Peng et al. 2000). Upper limits of dynamical predictability (i.e., using numerical climate models) when sea surface temperature (SST) is known perfectly throughout the forecast season were shown to be high in the Dynamical Seasonal Predictability (DSP; Shukla et al. 2000a) and the Prediction of Climate Variations on Seasonal to Interannual Timescales (PROVOST; Palmer et al. 2000) Projects. High skill is best realized through ensemble forecasts (Kumar et al. 2001). The main source of skill in winter ensemble climate forecasting comes from the El Niño/La Niña variations in the tropical Pacific (Shukla et al. 2000a).

Dynamical seasonal predictability derived from SST variations appears to be lower in other seasons (Anderson et al. 1999). However, there are examples of evidence for SST contributions to climate anomalies during the boreal warm season (Mo et al. 1991; Lau and Peng 1992; Trenberth and Branstator 1992; Trenberth and Guillemot 1996). The land surface has also been implicated in summer climate anomalies (Atlas et al. 1993; Beljaars et al. 1996; Paegle et al. 1996; Fennessy and Shukla 1999; Dirmeyer 2000; Douville 2002).

Previous studies have largely concentrated on anomalies related to specific case studies, or, at their broadest, on interannual variability during a single season. In this paper, a systematic comparison of seasonal climate predictability is performed among all seasons. There is no a priori reason to discount or exclude any season from an assessment of predictability, and relative roles of SST and soil moisture in providing seasonal forecast skill likely vary among seasons in interesting ways. After all, climate forecasting is not a seasonal sport but is performed operationally year-round. Comparisons are also made between seasonal integrations in the DSP vein and multidecadal simulations that span the same period, to isolate the influence of initial conditions from boundary conditions. This part of the investigation will also reveal the magnitude and structure of long-term climate drift in the coupled land–atmosphere model, and help to reveal its impact on climate predictability.

Section 2 describes the climate model and the various sets of numerical integrations. Section 3 discusses the results of the comparison between experiments and

Corresponding author address: Dr. Paul A. Dirmeyer, Center for Ocean–Land–Atmosphere Studies, 4041 Powder Mill Rd, Ste. 302, Calverton, MD 20705-3106.
E-mail: dirmeyer@cola.iges.org

TABLE 1. Description of the model integrations used in this study.

	DSP(OI)	DSP(HAD)	DSP-LIC	DSP-SST	C20C	AMIPII
Resolution	T63 (1.9°)	T63 (1.9°)	T63 (1.9°)	T63 (1.9°)	T63 (1.9°)	R40 (2.8° × 1.8°)
Ensemble size	10	10	10	10	10	7
SST	OI (Reynolds and Smith 1994)	HAD (Rayner et al. 1996)	OI	OI, but jumbled relative to ICs	HAD	OI
Atmosphere initial conditions	Late Feb, May, Aug 1982–99; late Nov 1981–98	Late Feb, May, Aug 1982–99; late Nov 1981–98	Late Feb, May, Aug 1982–99; late Nov 1981–98	Late Feb, May, Aug 1982–99; late Nov 1981–98	10–19 Nov 1948	1 Jan 1979
Land initial conditions	Climatological	Climatological	GOLD (realistic)	Climatological	Climatological	Climatological
Duration	4 months	4 months	4 months	4 months	50 yr	20 yr

among seasons. Section 4 focuses on the unique traits found for the boreal winter season. Conclusions are presented in section 5.

2. Model and experiments

The climate model used in all experiments consists of the Center for Ocean–Land–Atmosphere Studies (COLA) GCM, documented by Kinter et al. (1997), with the most recent version described by Schneider (2002). It is a research version of the global spectral model described by Sela (1980). The land surface is represented by an updated version of the simplified Simple Biosphere model (SSiB; Xue et al. 1991) as described by Dirmeyer and Zeng (1999). The COLA GCM skill in seasonal integrations has been shown in previous work (Shukla et al. 2000a,b). There are other seasonal studies that show the sensitivity of the climate of this model to soil wetness anomalies (Dirmeyer 2000), and the COLA GCM land state sensitivity has also been shown not to be extreme when compared to that of other models (Koster et al. 2002). Table 1 gives a summary of the various experiments described in this paper, which are detailed below.

The seasonal ensemble hindcasts were generated by the COLA GCM following the guidelines of the DSP project (Shukla et al. 2000a). Ensembles of 10 integrations at a resolution of T63 (1.875°) were completed for 18 consecutive years for each of the seasons. For winter, the atmospheric states of the integrations are initialized in late November 1981–98 and integrated forward for 4 months. Spring, summer, and autumn simulations are also for 4 months each, beginning in 1982–99, and initialized at the end of February, May, and August, respectively. In each season, five of the ensemble members are initialized from the 0000 UTC National Centers for Environmental Prediction–National Center for Atmospheric Research (NCEP–NCAR) global reanalyses (Kalnay et al. 1996) on the last 5 days of the month. The initial atmospheric states for the other five members are produced by perturbing the 0000 UTC states based on the differences between the bracketing 1200 UTC NCEP reanalyses.

The initial land surface states (soil moisture and temperature) are taken from the annual mean climatology of a 21-yr offline integration of the same land surface model as used in the COLA AGCM, referred to as the Global Offline Land-Surface Dataset (GOLD; Dirmeyer and Tan 2001). The procedure is very similar to that of the Global Soil Wetness Project (Dirmeyer et al. 1999) in that the land surface model is driven by 6-hourly NCEP reanalysis surface data that has been corrected by scaling so that the monthly means of precipitation, near-surface air temperature, and downward shortwave and longwave radiation agree with observationally based gridded datasets (Xie and Arkin 1997; Stackhouse et al. 2000). Relative humidity, winds, and surface pressure are not corrected. The offline integration is performed at the same resolution as the GCM and produces a global dataset of land surface state variables, from which a climatology is calculated for producing optimal initial conditions for GCM simulations. Thus, there is no interannual variability in the land initial conditions except in the DSP-LIC simulation, which uses the GOLD soil wetness states from each year. Similarly, initial snow cover is set from a climatology derived from a land albedo dataset (Kinter et al. 1997). Over ocean, boundary conditions of SSTs are specified from the weekly analysis of Reynolds and Smith (1994).

Data from two other ensembles of multidecade climate simulations are also examined in this paper. The COLA ensemble submission to the second Atmospheric Model Intercomparison Project (AMIP II; Gates et al. 1999; Gleckler 1996) has been used. The AMIP II ensemble consists of seven integrations at R40 resolution (1.8° latitude by 2.8° longitude) spanning the years 1979–98. To construct the ensemble, a single spinup run was performed, starting at 0000 UTC 1 January 1977 using the same initialization procedure described above. Upon integration to 0000 UTC 1 January 1979 (a period of 2 yr), the land surface conditions are then used to initialize all seven integrations. Each ensemble member has a unique initial atmospheric state taken from NCEP reanalyses at 0000 UTC from the days surrounding 1 January 1979. SSTs are specified from version 2.2 of the Hadley Centre Global Sea Ice SST

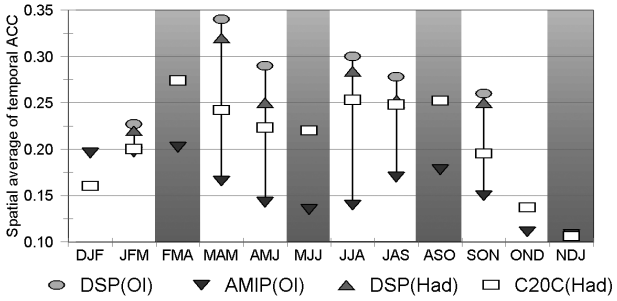

FIG. 1. Skill of seasonal mean hindcasts of global surface temperature over land (see text for definition) for seasonal DSP simulations with OI SST (ovals), HadISST (light triangles), AMIP II simulations with OI SST (dark triangles), and C20C simulations with HadISST (boxes).

(GISST2.2) dataset (Rayner et al. 1996) for the period 1979–81. Thereafter, SSTs were taken from the weekly analysis of Reynolds and Smith (1994), and are identical to that of the DSP runs. The AMIP II ensemble differs from the DSP ensemble in two important ways. It is performed with a lower-resolution version of the COLA GCM and has different settings in the cloud radiation parameterization.

COLA GCM ''Climate of the 20th Century'' (C20C; http://www.iges.org/c20c/) simulations at T63 resolution are also used. These consist of an ensemble of 10 integrations initialized at 0000 UTC 10–19 November 1948 using specified monthly Hadley Centre Global Sea Ice and SST [HadISST; a later version of the GISST data of Rayner et al. (1996)] analysis boundary conditions, and are integrated through 1998. The land surface initialization is identical to the DSP simulations. Except for the duration and the SST boundary conditions, the runs are not different than the DSP simulations. However, a parallel set of DSP simulations that use the same HadISST ocean temperatures as the C20C runs but are otherwise identical to the DSP simulations are also examined. These are distinguished when necessary by the name DSP(HAD), as opposed to DSP(OI) for the original seasonal hindcasts.

3. Results

In order to quantify the skill of the coupled land–atmosphere model in simulating the interannual variations of seasonal climate, we calculate at each grid point the anomaly correlation coefficient (ACC) between observed and modeled near-surface air temperatures. Anomalies for observations are relative to the mean for the 18-yr period 1982–99 [Climate Anomaly Monitoring System (CAMS); Ropelewski et al. 1985], and anomalies for the model are calculated for the ensemble mean of each year relative to the model's mean over the same 18 yr. Global averaged values of these temporal ACCs are calculated over land grid points between 60°S and 80°N.

Figure 1 compares the global averages of the temporal ACC for the 3-month seasons that are covered by the DSP simulations. Results are shown for the multidecade C20C and AMIP II ensemble integrations for all 3-month intervals, as well as for the DSP(OI) and DSP(HAD) seasonal ensembles. ACC is calculated on the ensemble mean in each case. There are two values for DSP during spring and summer, as 4-month simulations (March–June and June–September) were performed for those seasons. There is a marked difference in the skill of the DSP and C20C simulations across the year, with the DSP simulations consistently outperforming the C20C simulations. The difference is smallest during the boreal winter and largest during the equinoctial seasons. A difference of correlations of 0.04 is significant at the 90% level, 0.05 at the 95% level, and 0.07 at the 99% level, based on Student's t test with 120 spatial degrees of freedom over land (excluding Antarctica). Thus the variations during winter among the experiments are not discernable from noise, but the spread in the other seasons is significant, suggesting that the DSP simulations are genuinely superior to the C20C and AMIP II simulations for the same periods. The skill of the AMIP II simulations is particularly low. This may be due to the lower resolution of the AMIP II integrations or the different choice of physics. We include it in this comparison despite these fundamental differences because of the remarkably comparable skill these runs show during winter. Another feature of Fig. 1 is that for the DSP and C20C simulations in particular, skill is lowest during winter (OND–JFM). In most studies of atmospheric variables such as 500-hPa height, skill in seasonal predictions has been found to be highest during winter. The differences in predictability and skill between winter and the other seasons are discussed later in this paper.

Figure 2 shows the global distribution of the temporal anomaly correlation coefficients for months 1–3 [March–April–May (MAM)] and months 2–4 [April–May–June (AMJ)] from the DSP(OI) simulation. There are large spatially coherent regions of high correlation. These regions change from month to month and from season to season (not shown). It is also evident in both panels of Fig. 2 that during spring and summer there is a drop in skill within the DSP simulations from months 1–3 (MAM and JJA) to months 2–4 (AMJ and JAS). This is a reflection of the loss of information from the initial atmospheric state over the course of the first month. During the first month of the DSP simulations, the persistence of the anomalies in the initial state of the atmosphere, which is prescribed from observations, provides some predictive inertia in the dynamical and thermodynamic quantities.

This is more clearly evident when we examine the data month by month. Figure 3 shows the progression of the global mean temporal ACC from June through September for the boreal summer DSP simulations. Also shown are results from an additional set of simulations where the atmospheric initial conditions and specified

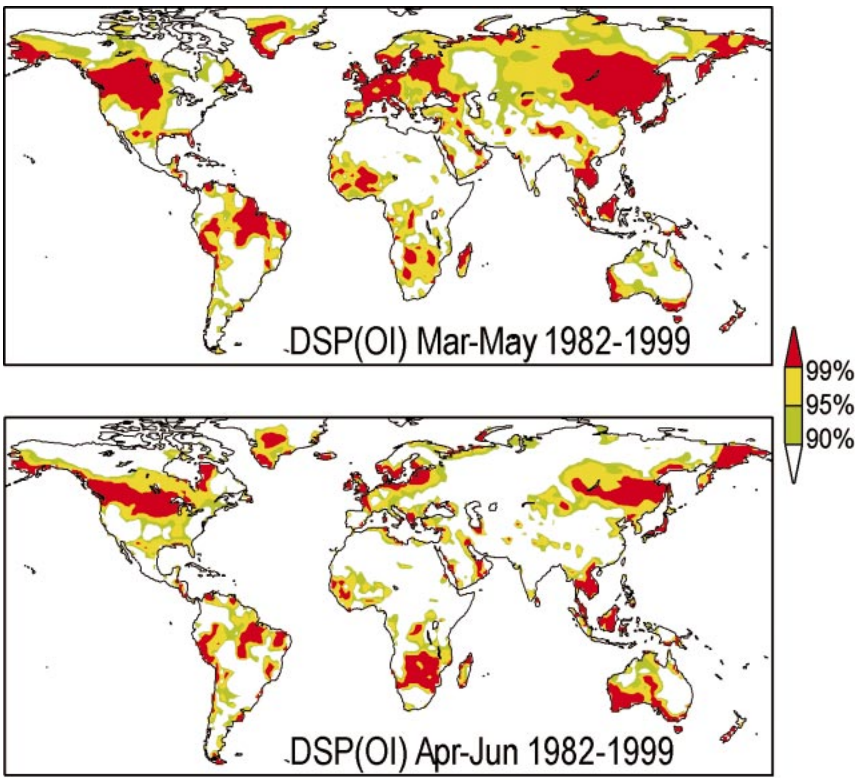

FIG. 2. Global distribution of the temporal anomaly correlation coefficients for surface temperature over land during (top) months 1–3 and (bottom) months 2–4 from the spring DSP (OI) simulation. The significance levels of 90%, 95%, and 99% correspond to ACCs of 0.32, 0.40, and 0.54, respectively.

SST are shuffled relative to one another (DSP-SST). By validating the results of this set against the observations for the year corresponding to the chosen initial conditions, we can see the role of the initial conditions in the skill of the temperature forecasts. Likewise, by pairing the observations with the runs based on the year of the specified SST, we can assess the ocean's role in the skill of temperature simulation over land.

The ACCs for the case synchronized to initial conditions are connected by a solid line. The skill during the first month is higher than for the case with correct SST but incorrect atmospheric initial conditions. Over the course of the first month, the atmospheric initial condition is very important to the overall skill of the forecast. However, by month 2 (July), the skill afforded by the initial atmospheric state has dropped well below that derived from the observed SST, and by months 3 and 4 there is no skill originating from correct knowledge of the initial atmospheric state. During months 2–4 (July–September), essentially all of the skill in the control DSP simulation appears to be derived from the specification of the SST. Similar results are found for spring seasons (not shown). This is consistent with previous research on the upper limits of predictability derived from the initial state in the medium-range to seasonal timescale (e.g., Shukla 1985; Chen 1989; Schubert et al. 1992).

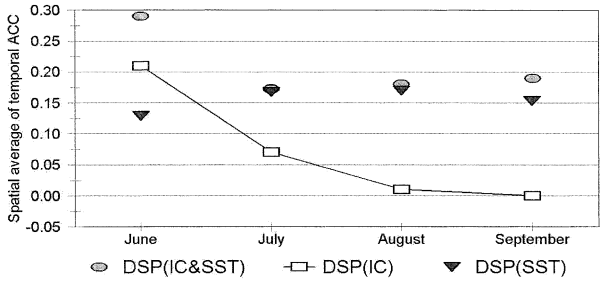

FIG. 3. Evolution of skill in seasonal hindcasts of global surface temperature with late May initial conditions (ovals); and the skill derived from atmospheric initial conditions (boxes) and specified SST boundary conditions (triangles).

To ensure that ACCs found in the DSP simulations are robust, we also show results for 850-hPa temperature (Fig. 4). Here comparisons are made to the anomalies found in the NCEP–U.S. Department of Energy (DOE) reanalyses (Kanamitsu et al. 2002). Globally averaged temporal ACC is systematically higher over land for 850-hPa temperature than for near-surface temperature for all seasons, and it fluctuates across the annual cycle in the same fashion. The difference in skill may reflect the surface temperature errors introduced by shortcom-

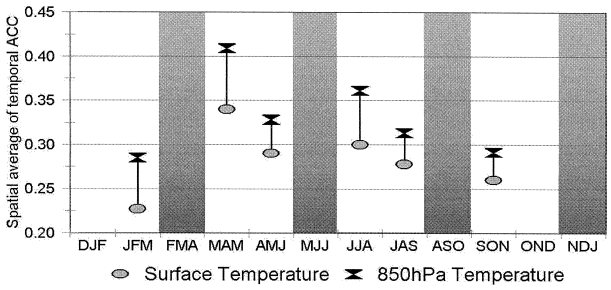

FIG. 4. As in Fig. 1, but for near-surface air temperature (ovals) and 850-hPa temperature (hourglasses) from the DSP simulations with OI SST.

ings in the land surface scheme, or it could be due to the fact that different datasets were used for validation. The 850-hPa temperature fields are also smoother than the surface fields, so degradation in the skill statistic from small-scale noise may also be reduced. Nevertheless, the behavior of the lower-tropospheric and surface temperatures appears to be consistent, and the skill statistics robust.

We can see from Fig. 1 that, regardless of the loss of impact of the atmospheric initial state to the DSP simulations by the second month, those simulations are still superior to the C20C ensemble, which uses identically the same model at the same resolution. However, they do use different SST datasets. For clearer comparison, the DSP simulations were repeated with the same monthly HadISST data as used in the C20C simulations (light triangles in Fig. 1). There is some apparent reduction in skill compared to DSP(OI) but the globally averaged temporal ACC is still consistently higher than for the C20C simulations. Thus, it is clear that the difference in skill between the DSP and C20C simulations cannot be attributed completely to the choice of SST dataset or the influence of atmospheric initial conditions on the DSP simulations.

The only other element of the coupled model system that could be fundamentally different between the DSP and C20C simulations is the land surface state. Like the ocean, the land surface is a slowly varying boundary condition to the atmosphere. However, the memory in the land comes predominantly from hydrologic quantities rather than heat capacity. Soil moisture and snow cover provide the inertia over land. However, that inertia is on the order of months (Schlosser and Milly 2002). The AMIP II simulations are from 3 to 20 yr beyond their atmospheric and land surface initialization. The C20C simulations are several decades beyond their initial conditions.

A previous study documented the impact of climate drift on coupled land–atmosphere simulations on the daily to seasonal timescale (Dirmeyer 2001). The systematic drift described there can continue to grow well beyond the seasonal timescale. Figure 5 shows the drift in soil moisture in the C20C simulations over a portion of North America corresponding approximately to the contiguous United States, compared to that in the DSP simulations and the soil wetness climatology used to initialize all of the GCM simulations. Running 3-month means are shown for the C20C integration and clima-

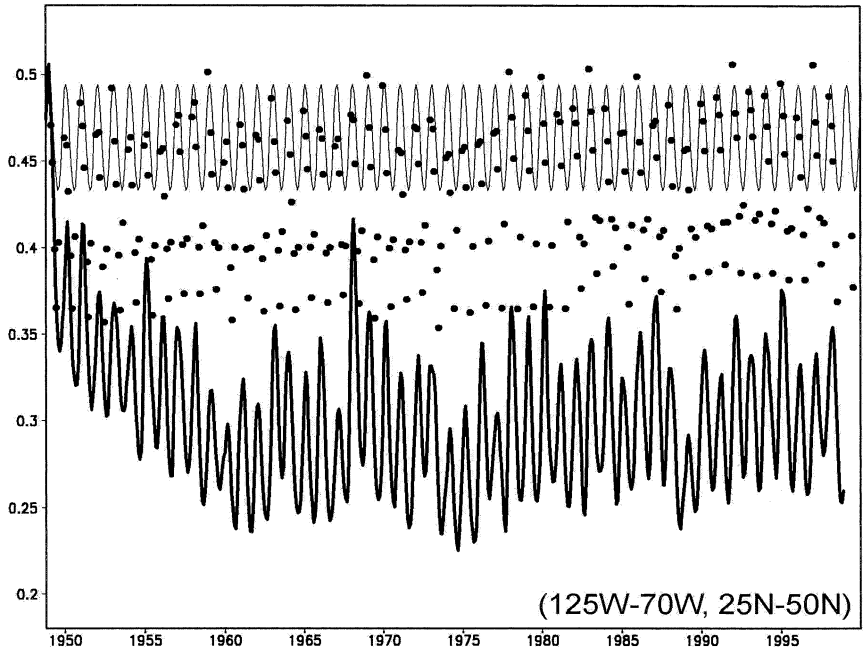

FIG. 5. Area average 3-month mean of root zone soil wetness for DSP simulations (dots); C20C simulations (bold curve); and climatological initial soil wetness used in all simulations (thin curve).

tology. Because the DSP simulations are 3–4 months in duration, only the 3-month means that can be calculated from continuous integrations are shown.

There is a clear drying phase during the first decade of the C20C simulation. During this period, the C20C root zone soil wetness drops by one third, from about 0.45 ± 0.05 to 0.30 ± 0.05 [c.f. Fig. 3 of the Roads et al. (1999) analysis for the NCEP GCM]. The envelopes of soil wetness between C20C and DSP simulations show almost no overlap. The DSP simulations are generally drier than the climatological initialization, particularly during the warm seasons. This reflects the drift that occurs on the seasonal timescale. In fact, drift sets in immediately after the start of any integration (e.g., the steep slope during the first few years of the C20C simulation, which is particularly sharp during the first boreal summer) and levels off as the erroneous coupled equilibrium is reached. So the DSP results exhibit some drift in soil wetness but are not long enough for the drift to attain the degree found in the later years of the C20C simulations.

The cause for this drift is clear when one examines the systematic errors in the downward fluxes of energy and water at the surface. In a previous paper, Dirmeyer (2000) showed a strong correlation between the spatial pattern of climate drift in soil wetness and systematic errors in GCM precipitation and downward shortwave radiative flux at the land surface. These errors for the boreal summer season (June–August), averaged over the 1982–99 seasons, are shown in Fig. 6, along with errors in downward longwave radiation. Precipitation is validated against the observational analysis of Xie and Arkin (1997); radiation fields are compared to the surface radiation budget products of Stackhouse et al. (2000). Values are not shown over either ocean or permanent ice cover.

Overall there is a wet bias in precipitation over land in the climate model, with positive anomalies widespread at high latitudes. In the Tropics and monsoon regions there is a mixture of strong positive and negative biases. The tropical rainfall belt over Africa is too intense and narrowly confined in latitude. The Indian, southern Indochinese, and eastern Chinese portions of the Asian monsoon are too dry, with wet biases elsewhere in the region, including Indonesia. Southern Mexico, Central America, and the core of the Amazon basin are too wet, while the western Amazon basin, northern Mexico, and the southern United States are dry.

Errors in downward longwave radiation at the land surface are much more coherent. There is a strong correspondence between negative anomalies in downward longwave radiation and the location of semiarid and arid regions. The strongest negative biases are over the deserts of Arabia and central Asia. The COLA AGCM has no treatment of aerosols in its radiative parameterization. There is some attenuation of radiation by water vapor and, of course, by cloud. The errors in longwave radiation suggest a potential problem caused by the lack of dust in the model, which might otherwise absorb upwelling longwave radiation and increase lower-tropospheric temperatures over deserts (Alpert et al. 1998).

Errors in downward shortwave radiation at the surface are positive nearly everywhere, and are particularly large over the Asian and North American monsoon regions. However, there are positive errors of at least 20 W m^{-2} throughout the Northern Hemisphere over land. This may again implicate the lack of aerosols in the model, or perhaps more fundamentally the parameterization of clouds and their interaction with solar radiation.

Whatever the causes, the result of these errors is that there is a net excess in the downward fluxes of both radiative energy and water over land. Locally, there may be an excess or a deficit of water and likely an excess of energy outside of the deserts. An abundance or deficiency of precipitation will directly lead to a similar bias in soil wetness, in the presence of constant evaporation. But biases in downward radiation alter the amount of energy available for evaporation, so these proclivities can also skew the local water budget. Whereas energy and water budgets are balanced locally at the land–atmosphere interface regardless of the downward fluxes, the large biases may lead to either excessive or insufficient drying of the surface. Over time, this drives the soil wetness to an extreme state: either excessively wet or dry, depending on the nature of the errors.

Figure 7 illustrates this effect on the seasonal scale. The top panel shows the sum of the errors in Fig. 6, converting precipitation into a latent heat sink by multiplying the water mass by negative of the latent heat of condensation. Colors on the red side of the spectrum indicate a net error on the side of excessive energy or insufficient water—a drying effect. Blue colors indicate a shortfall of energy or overabundance of water. In the net, drying predominates. The northern high latitudes receive excess rainfall and shortwave radiation, but Fig. 7 suggests that the radiation errors predominate. Desert regions receive a net shortfall of downwelling energy mainly due to the longwave errors, but rainfall is nearly zero, so impacts on the surface water budget are minimal. Only at low latitudes can positive rainfall errors overwhelm the biases in downward radiative fluxes.

The lower panel of Fig. 7 shows the drift in root zone soil wetness (measured as a value of 1.0 when soil is saturated, 0.0 when completely desiccated) after 3 months of simulation, as compared to the climatology used to provide the initial conditions. The correspondence between the two panels is very high ($r = 0.71$). Recall that the same land surface model is used in the climate simulations as well as to calculate the soil moisture climatology (from forcing data derived from observations and atmospheric reanalysis). Thus, this comparison cannot elucidate errors in the land surface model itself. It does, however, suggest that the cause of the drift is the differences between the meteorological ob-

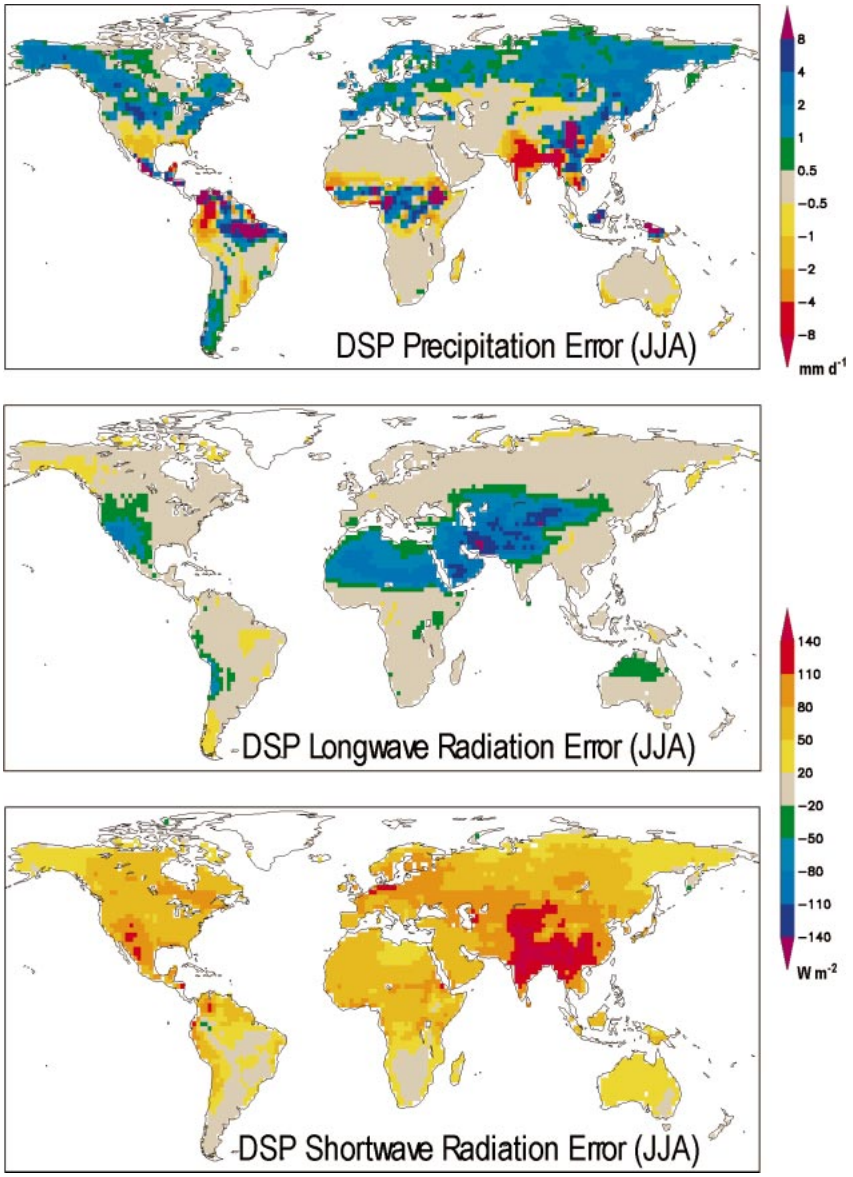

FIG. 6. (top) Errors in DSP summer season precipitation rate; (middle) downward longwave radiation at the surface; and (bottom) downward shortwave radiation at the surface.

servations of energy and water fluxes at the surface and the corresponding downward GCM fluxes passed between the atmosphere and land components of the climate model.

This is even more evident at longer timescales. The top panel of Fig. 8 shows the August soil wetness over the contiguous United States, averaged over the last 20 yr of the C20C simulation (1979–98). This is a period that corresponds almost exactly with that of the GOLD soil wetness product from which the initial conditions were generated. The bottom panel shows the drift relative to the August climatological GOLD root zone soil wetness. Almost complete desiccation has occurred, with only New England and the northern Rocky Mountains showing an appreciable wet bias. These features are in general agreement with the patterns evident in Fig. 7.

Even more disconcerting is the fact that virtually none of the area has a soil moisture bias near zero. Over the course of a half-century integration, the soil moisture has largely drifted to extreme dry and wet states. This is problematic because sensitivity of upward surface fluxes (i.e., the partitioning of available energy between sensible and latent heat fluxes) to fluctuations in soil wetness is greatest when soil moisture is in the middle range between wilting point and field capacity. This is the basis of the β formulations for estimating evapotranspiration (e.g., Sud and Fennessy 1982). When the

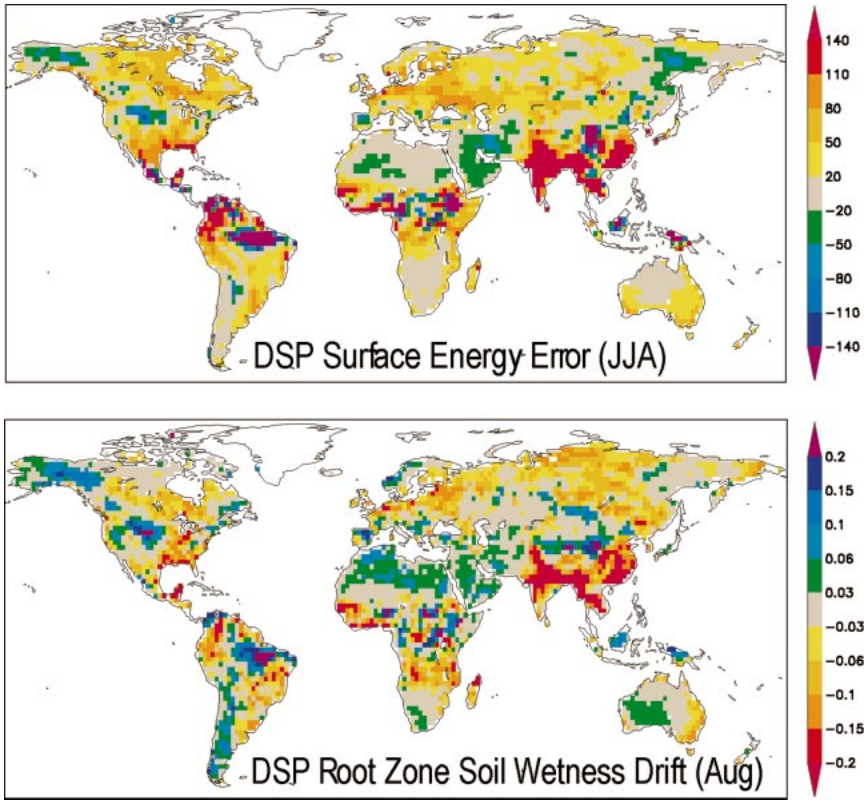

FIG. 7. (top) Error in total mean summer surface energy (downward radiative energy minus energy required to evaporate all precipitation, in W m^{-2}); (bottom) error (relative to GOLD) in ensemble mean soil wetness in the root zone averaged over all DSP simulations for Aug.

soil is relatively wet, evaporation and transpiration can occur near their potential rates. Perturbations have little effect on these fluxes, and the Bowen ratio remains low. On the other hand, when soil is extremely dry, conductivity of water in the soil is very low. Vegetation is stressed and does not transpire, and evaporation from the soil is very low. Again, a small or moderate perturbation will not greatly affect evapotranspiration, and the Bowen ratio remains high. Maximum sensitivity occurs where the rate of change of evapotranspiration with a change in soil moisture is greatest, in the middle of the range. Figure 9 shows the distribution of monthly mean latent heat fluxes as a function of soil wetness for the specific case of grassland with medium soil texture (mixing vegetation and soil types convolutes the relationship by mixing curves that separately exhibit distinct sensitivity bands). The slope of $\delta\lambda/\delta w$, where λ is latent heat flux and w is root zone soil wetness, is maximum for moderate soil wetness, and flattens out at the tails. This is the range where there would be maximum sensitivity of evaporation to a soil wetness perturbation of a given magnitude δw.

The result of this land surface drift is that the climate model becomes largely insensitive to interannual variations in soil wetness. Perturbations on the drifted background state cannot induce much of a response in surface fluxes, and the positive feedback mechanism that could amplify the climate response is suppressed. In addition, the same systematic errors in the fluxes from the atmospheric model are still in place, preventing a recovery from the drifted state.

4. The winter singularity

Referring back to Fig. 1, we noted that the spread among the various experiments is smallest during boreal winter. It appears that during boreal winter, the surface soil moisture state is uniquely unimportant for climate prediction.

This is illustrated in Fig. 10, which shows the square root of the zonal mean (land only) interannual variance in seasonal mean surface latent heat flux taken from the DSP(HAD) simulations. It is expressed in terms of a standard deviation multiplied by the land area in each zonal band (a total flux in watts), to emphasize the larger potential impact of terrestrial latent heat flux variability at latitude bands that have a large land mass. At most latitudes in the Northern Hemisphere, the weakest interannual variability is during winter; the strongest is during summer, followed closely by spring. Results are similar for sensible heat flux (not shown), except that fall is the season of weakest interannual variability at

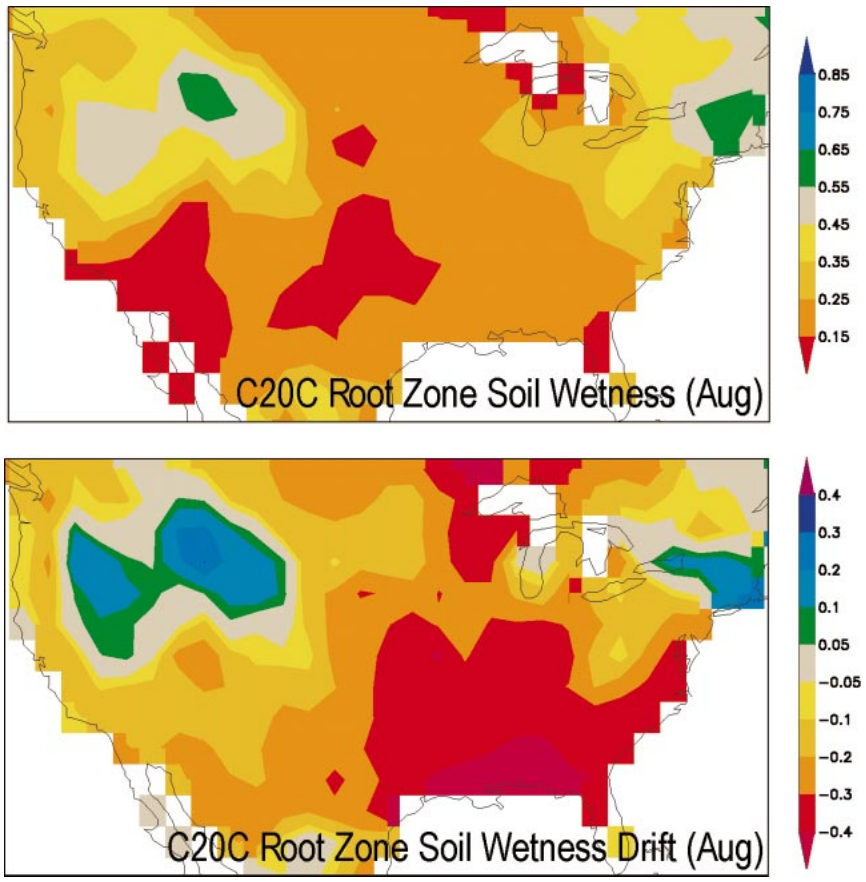

FIG. 8. (top) Aug mean root zone soil wetness averaged over the last 20 yr of the C20C simulations; (bottom) difference between top panel and climatological (GOLD) Aug root zone soil wetness for the same period. The region shown is the same as that averaged in Fig. 3.

most latitudes. Since the climate response to land surface variations is largely confined to the region of the anomalies, and the majority of land surface area is in the Northern Hemisphere, we expect the global signals portrayed in Fig. 1 to be dominated by events in the Northern Hemisphere. Thus we have confined the plot to north of the equator. Figure 10 shows that interannual

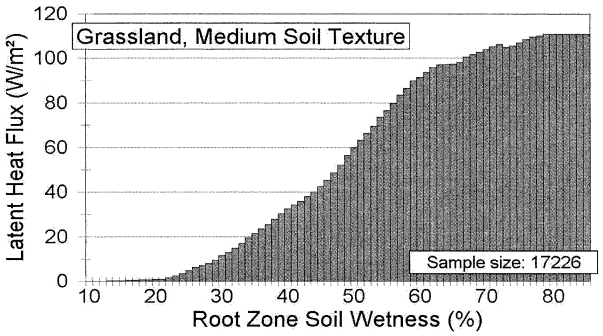

FIG. 9. Ensemble mean monthly latent heat flux rate as a function of root zone soil wetness during boreal summer for all years of the DSP simulations at grassland grid points with medium soil texture.

variability of surface energy fluxes from land to atmosphere is at a minimum during boreal winter.

Boreal winter seems to be a unique time of year, in that during this one season several global-scale events conspire to give sea surface temperature a singular role in determining a sizeable fraction of the observed climate variability. The general circulation of the Northern Hemisphere becomes most favorable for supporting teleconnections from the Tropics (Horel and Wallace 1981). At the same time, the El Niño–Southern Oscillation (ENSO) reaches its maximum amplitude, providing an anomaly in tropical heating to excite the teleconnection pattern (Rasmusson and Carpenter 1982). And as shown in this study, the role of the land surface in inducing seasonal climate variations is most inhibited. This inhibition may also be due to the superposition of multiple factors. As shown, there exists an annual minimum in surface heat flux variability. During winter, much of the land surface of the earth, predominantly in the Northern Hemisphere, is under the influence of strong baroclinic wave activity and is relatively uncoupled from the atmosphere (Viterbo and Beljaars 2002). Also, subtropical regions of the Northern Hemisphere

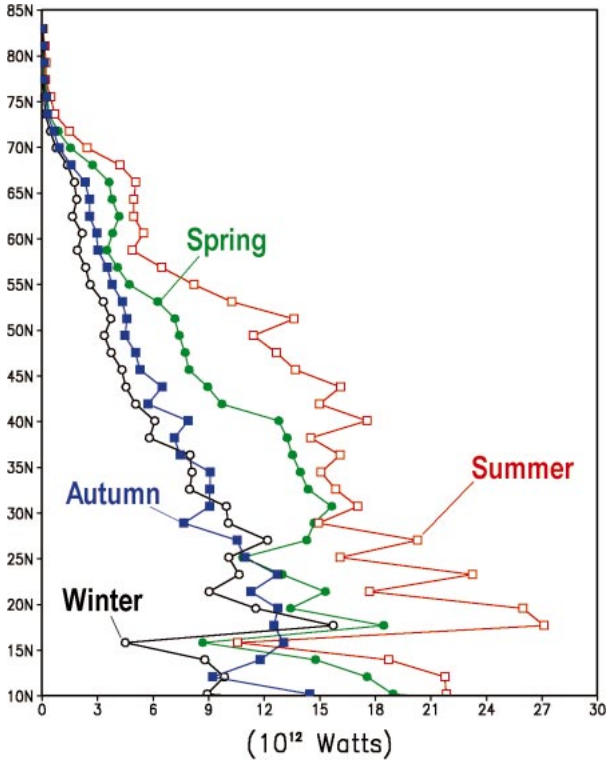

FIG. 10. Square root of zonal total interannual variance of seasonal mean latent heat flux over land points as a function of latitude and season.

are in their dry seasons, and interannual variability of surface energy fluxes (latent and sensible heat) are at a minimum.

5. Remarks and conclusions

For all seasons except boreal winter, the skill of ensemble mean dynamical seasonal (DSP) hindcasts of terrestrial surface temperature anomalies produced by a general circulation model with observed oceanic boundary conditions is significantly better than for simulations for the same seasons taken from long integrations that were initialized many years earlier (AMIP II or C20C). Identical models were used in all cases, with the identical climatological initialization procedure for the land surface, and atmospheric initialization based on NCEP reanalyses. Differences exist in the SST datasets used in some of the cases, but these variations were found to have minimal impact on the result. The AMIP II integrations have more potentially consequential differences from the other cases, including a lower spatial resolution and different settings for the cloud radiation parameterization.

Boreal spring and summer DSP simulations of 4 months duration have two separate 3-month seasonal means calculated—one from months 1–3 and another from months 2–4. It is found that the predictability contributed by the atmospheric initial conditions provides a boost to skill only during the first month. Nevertheless, skill for DSP hindcasts from months 2–4 are still significantly higher than from the corresponding seasons taken from C20C or AMIP II simulations. The skill that is present in predicting interannual anomalies over land in the long simulations can only originate from the specified SST—there is no other source of specified year-to-year variability, and the simulations are too long to treat the predictions as a solvable initial value problem in the coupled land–surface atmosphere system.

The culprit implicated in this difference of skill is the state of the modeled land surface, specifically soil wetness, which undergoes a profound drift over time. Thus, the background state of the land surface in the long simulations is considerably different than that in the DSP simulations. The background state of the land surface appears to be important for the realization of the effects of SST variability on climate over land.

The effect of climate drift in the coupled land–atmosphere model is twofold. First, the strong drift in the first months of an integration (particularly during the boreal warm season) can potentially overwhelm any potential signal in the land surface initial conditions, such as a soil wetness anomaly. The seasonal hindcasts presented here all start from climatological initial land conditions, but a companion set of simulations with realistic initial land surface conditions that include interannual variations (DSP-LIC; again taken from the GOLD analysis), not discussed in this paper, shows no appreciable difference in skill compared to the control runs. It may be that correction of the drift, whether by improved parameterizations of atmospheric physics, better calibration of existing parameterizations, or a statistical approach to mean error reduction will improve the model's skill at seasonal prediction. Other simulations with an earlier version of this model that had less climate drift (Dirmeyer 2000), as well as experiments using other models (e.g., Fennessy and Shukla 1999; Douville 2002) suggest that a correct land surface state can improve predictive skill in climate models.

Second, in long simulations the drift carries the soil moisture to extreme states. These fully drifted land states appear to hamper the skill of the climate model in simulating the response of climate to observed SST variability. Comparisons between the DSP, AMIP II and C20C simulations show that while the initial atmospheric conditions afford some skill to the forecasts during the first month, the DSP simulations are still significantly superior during months 2–4. This can be seen in Fig. 11, which presents the same monthly skill measures for the boreal summer DSP simulations as in Fig. 3, but compares them to the AMIP II and C20C simulations. The AMIP II simulations still show the lowest skill, perhaps for the reasons outlined in section 3. However, there is a clear inferiority of the C20C simulations compared to DSP.

The singular state of boreal winter is shown by the

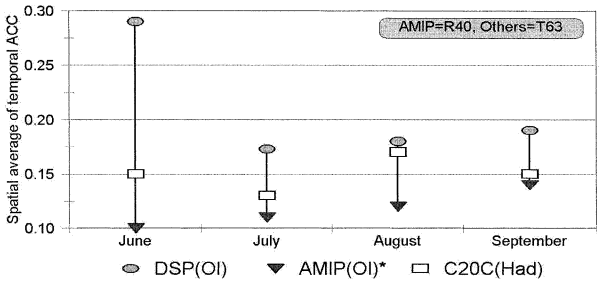

FIG. 11. As in Fig. 2 for the control DSP simulation and the two multidecadal simulations.

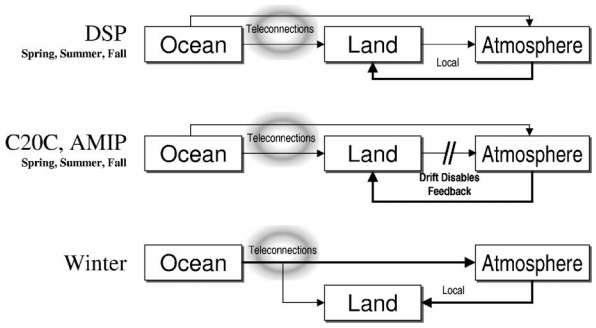

FIG. 12. Schematic of teleconnections and feedbacks in the ocean–atmosphere–land system as manifest in the climate model.

insensitivity of climate simulations to the state of the land surface, the degree of spinup of the model, resolution, or differences in some model parameterizations. During boreal winter, interannual variability of tropical SST is largest, manifest in the El Niño phenomenon, while interannual variability in land surface heat fluxes is smallest. The tropical and extratropical circulations are most favorable for transmitting the signal of tropical heating anomalies into the Northern Hemisphere extratropics, where most of the planet's land surface lies. Also, the strong baroclinic nature of the extratropical troposphere during winter acts to decouple the land surface from the atmosphere. The cumulative result is the minimization of the role of land surface variability and a maximization of the role of ocean variability on global terrestrial climate.

Figure 12 schematically portrays the variations found among the different climate simulations and seasons. In the DSP simulations during spring, summer, and fall, remote SST anomalies affect the climate over land (atmosphere and land surface) via teleconnections through the intervening troposphere. The feedback between land (soil moisture and temperature) and atmosphere (precipitation and temperature) is generally positive and helps to reinforce anomalies and support predictability of interannual variations. Drift in the local coupled land–atmosphere part of the system is beginning but has not had a catastrophic impact on the feedback loop. In the case of the C20C and AMIP II simulations, the drift has occurred over a sufficiently long time that soil moisture over much of the globe is in an extreme dry or wet state. The mechanism for perturbations at the land surface to induce atmospheric variations has largely been lost, and the feedback loop is broken. This situation is tantamount to running an atmospheric model without an interactive land surface. The bottom schematic depicts the situation during boreal winter. The direct effect of remote SST anomalies on the troposphere over land is strongest, and the land surface has little impact on the atmosphere. The breakdown of the land–atmosphere feedback loop in the C20C and AMIP II runs is of little consequence over much of globe during boreal winter, and the GCM shows similar skill in all cases.

In the DSP simulations, the land surface feedback has a positive impact on predictive skill, and helps lead to greater skill scores for surface temperature than are realized during winter (see Fig. 1). The conventional wisdom in seasonal forecasting is that the best prospects for skill reside in boreal winter, and other seasons show poor prospects for useful predictability. These assertions have largely been based on metrics such as root-mean-square error of hemispheric 500-hPa geopotential height anomalies. This study suggests that for some quantities of more use to climate applications, there may be more potential predictability in seasons outside of winter. However, the key to unlocking this predictability may be in the ability of climate models to properly simulate the balance of fluxes and feedbacks between land and atmosphere.

Acknowledgments. The author produced only the summer DSP (OI) simulations, including the DSP-LIC and DSP-SST cases; most of the integrations were performed by others, including L. Marx [autumn and winter DSP(OI) and C20C], C. A. Schlosser [spring DSP(OI) and AMIP II], and D. Paolino [DSP(HAD)]. This work was conducted as part of omnibus research at the Center for Ocean–Land–Atmosphere Studies, supported by NSF Grant ATM 9814265, NOAA Grant NA96GP0056, and NASA Grant NAG5-8202.

REFERENCES

Alpert, P., Y. J. Kaufman, Y. Shay-El, D. Tanre, A. da Silva, S. Schubert, and J. H. Joseph, 1998: Quantification of dust-forced heating of the lower troposphere. *Nature,* **395,** 367–370.

Anderson, J., H. Van den Dool, A. Barnston, W. Chen, W. Stern, and J. Ploshay, 1999: Present-day capabilities of numerical and statistical models for atmospheric extratropical seasonal simulation and prediction. *Bull. Amer. Meteor. Soc.,* **80,** 1349–1362.

Atlas, R., N. Wolfson, and J. Terry, 1993: The effect of SST and soil moisture anomalies on GLA model simulation of the 1988 U.S. summer drought. *J. Climate,* **6,** 2034–2048.

Barnston, A. G., Y. He, and D. A. Unger, 2000: A forecast product that maximizes utility for state-of-the-art seasonal climate prediction. *Bull. Amer. Meteor. Soc.,* **81,** 1271–1280.

Beljaars, A. C., P. Viterbo, M. J. Miler, and A. K. Betts, 1996: The anomalous rainfall over the United States during July 1993: Sensitivity to land surface parameterization and soil moisture anomalies. *Mon. Wea. Rev.,* **124,** 362–383.

Chen, W. Y., 1989: Estimate of dynamical predictability from NMC DERF experiments. *Mon. Wea. Rev.,* **117,** 1227–1236.

Dirmeyer, P. A., 2000: Using a global soil wetness dataset to improve seasonal climate simulation. *J. Climate,* **13,** 2900–2922.
——, 2001: Climate drift in a coupled land–atmosphere model. *J. Hydrometeor.,* **2,** 89–100.
——, and F. J. Zeng, 1999: An update to the distribution and treatment of vegetation and soil properties in SSiB. COLA Tech. Rep. 78, 25 pp. [Available from the Center for Ocean–Land–Atmosphere Studies, 4041 Powder Mill Road, Suite 302, Calverton, MD 20705.]
——, and L. Tan, 2001: A multi-decadal global land-surface data set of state variables and fluxes. COLA Tech. Rep. 102, 43 pp. [Available from the Center for Ocean–Land–Atmosphere Studies, 4041 Powder Mill Road, Suite 302, Calverton, MD 20705.]
——, A. J. Dolman, and N. Sato, 1999: The Global Soil Wetness Project: A pilot project for global land surface modeling and validation. *Bull. Amer. Meteor. Soc.,* **80,** 851–878.
Douville, H., 2002: Influence of soil moisture on the Asian and African monsoons. Part II: Interannual variability. *J. Climate,* **15,** 701–720.
Fennessy, M. J., and J. Shukla, 1999: Impact of initial soil wetness on seasonal atmospheric prediction. *J. Climate,* **12,** 3167–3180.
Gates, W. L., and Coauthors, 1999: An overview of the results of the Atmospheric Model Intercomparison Project (AMIP I). *Bull. Amer. Meteor. Soc.,* **80,** 29–55.
Gleckler, P., Ed., 1996: AMIP II guidelines. *AMIP Newsletter,* No. 8, PCMDI, Lawrence Livermore National Laboratory, Livermore, CA, 20 pp.
Horel, J. D., and J. M. Wallace, 1981: Planetary-scale atmospheric phenomena associated with the Southern Oscillation. *Mon. Wea. Rev.,* **109,** 813–829.
Kalnay, E., and Coauthors, 1996: The NCEP/NCAR 40-Year Reanalysis Project. *Bull. Amer. Meteor. Soc.,* **77,** 437–471.
Kanamitsu, M., W. Ebisuzaki, J. Woolen, S.-K. Yang, J. J. Hnilo, M. Fiorino, and G. L. Potter, 2002: NCEP–DOE AMIP-II reanalysis (R-2). *Bull. Amer. Meteor. Soc.,* **83,** 1631–1648.
Kinter, J. L., and Coauthors, 1997: The COLA atmosphere–biosphere general circulation model. Volume 1: Formulation. COLA Tech. Rep. 51, 46 pp. [Available from the Center for Ocean–Land–Atmosphere Studies, 4041 Powder Mill Road, Suite 302, Calverton, MD 20705.]
Koster, R. D., P. A. Dirmeyer, A. N. Hahmann, R. Ijpelaar, L. Tyahla, P. Cox, and M. J. Suarez, 2002: Comparing the degree of land–atmosphere interaction in four atmospheric general circulation models. *J. Hydrometeor.,* **3,** 363–375.
Kumar, A., A. G. Barnston, and M. P. Hoerling, 2001: Seasonal predictions, probabilistic verifications, and ensemble size. *J. Climate,* **14,** 1671–1676.
Lau, K. M., and L. Peng, 1992: Dynamics of atmospheric teleconnections during the northern summer. *J. Climate,* **5,** 140–158.
Mo, K. C., J. R. Zimmerman, E. Kalnay, and M. Kanamitsu, 1991: A GCM study of the 1988 United States drought. *Mon. Wea. Rev.,* **119,** 1512–1532.
Paegle, J., K. C. Mo, and J. Nogues-Paegle, 1996: Dependence of simulated precipitation on surface evaporation during the 1993 United States summer floods. *Mon. Wea. Rev.,* **124,** 345–361.
Palmer, T. N., C. Brankovic, and D. S. Richardson, 2000: A probability and decision-model analysis of PROVOST seasonal multimodel ensemble integrations. *Quart. J. Roy. Meteor. Soc.,* **126,** 2013–2033.
Peng, P., A. Kumar, A. G. Barnston, and L. Goddard, 2000: Simulation skills of the SST-forced global climate variability of the NCEP–MRF9 and the Scripps–MPI ECHAM3 models. *J. Climate,* **13,** 3657–3679.
Rasmusson, E. M., and T. H. Carpenter, 1982: Variations in tropical sea surface temperature and surface wind fields associated with the Southern Oscillation/El Niño. *Mon. Wea. Rev.,* **110,** 354–384.
Rayner, N. A., E. B. Horton, D. E. Parker, C. K. Folland, and R. B. Hackett, 1996: Version 2.2 of the global sea ice and sea surface temperature data set 1903–1994. Climate Tech. Res. Note 74, Hadley Centre, Bracknell, Berkshire, United Kingdom, 35 pp.
Reynolds, R. W., and T. M. Smith, 1994: Improved global sea surface temperature analyses using optimal interpolation. *J. Climate,* **7,** 929–948.
Roads, J. O., S.-C. Chen, M. Kanamitsu, and H. Juang, 1999: Surface water characteristics in NCEP global spectral model and reanalysis. *J. Geophys. Res.,* **104,** 19 307–19 327.
Ropelewski, C. F., J. E. Janowiak, and M. F. Halpert, 1985: The analysis and display of real time surface climate data. *Mon. Wea. Rev.,* **113,** 1101–1107.
Schlosser, C. A., and P. C. D. Milly, 2002: A model-based investigation of soil moisture predictability and associated climate predictability. *J. Hydrometeor.,* **3,** 483–501.
Schneider, E. K., 2002: The causes of differences between equatorial Pacific SST simulations of two coupled ocean–atmosphere general circulation models. *J. Climate,* **15,** 449–469.
Schubert, S. D., M. J. Suarez, and J.-K. Schemm, 1992: Persistence and predictability in a perfect model. *J. Atmos. Sci.,* **49,** 256–269.
Sela, J. G., 1980: Spectral modeling at the National Meteorological Center. *Mon. Wea. Rev.,* **108,** 1279–1292.
Shukla, J., 1985: Predictability. *Advances in Geophysics,* Vol. 28, Academic Press, 87–122.
——, and Coauthors, 2000a: Dynamical seasonal prediction. *Bull. Amer. Meteor. Soc.,* **81,** 2593–2606.
——, D. A. Paolino, D. M. Straus, D. DeWitt, M. Fennessy, J. L. Kinter, L. Marx, and R. Mo, 2000b: Dynamical seasonal predictions with the COLA atmospheric model. *Quart. J. Roy. Meteor. Soc.,* **126,** 2265–2291.
Stackhouse, P. W., Jr., S. K. Gupta, S. J. Cox, M. Chiacchio, and J. C. Mikovitz, 2000: The SRB Project Release 2 Data Set: An update. *WCRP GEWEX News,* Vol. 10, No. 3,4.
Sud, Y. C., and M. J. Fennessy, 1982: An observational-data based evapotranspiration function for general circulation models. *Atmos.–Ocean,* **20,** 301–316.
Trenberth, K. E., and G. W. Branstator, 1992: Issues in establishing causes of the 1988 drought over North America. *J. Climate,* **5,** 159–172.
——, and C. J. Guillemot, 1996: Physical processes involved in the 1988 drought and 1993 floods in North America. *J. Climate,* **9,** 1288–1298.
Viterbo, P., and A. C. M. Beljaars, 2002: Impact of land surface on weather. *Vegetation, Water, Humans and Climate: A New Perspective on an Interactive System,* M. Claussen et al., Eds., Springer-Verlag, 58–89.
Xie, P., and P. A. Arkin, 1997: Global precipitation: A 17-year monthly analysis based on gauge observations, satellite estimates, and numerical model outputs. *Bull. Amer. Meteor. Soc.,* **78,** 2539–2558.
Xue, Y., P. J. Sellers, J. L. Kinter, and J. Shukla, 1991: A simplified biosphere model for global climate studies. *J. Climate,* **4,** 345–364.